Meteoritics & Planetary Science 34, 959–968 (1999)

Activity of the 1998 Leonid shower from video records

PETER JENNISKENS

SETI Institute, NASA Ames Research Center, Mail Stop 239-4, Moffett Field, California 94035, USA
Author's e-mail address: peter@max.arc.nasa.gov

(Received 1999 June 8; accepted in revised form 1999 August 16)
(Presented at a Workshop on the Leonid Multi-Instrument Aircraft Campaign, Moffett Field, California, 1999 April 12–15)

Abstract–Video observations of the Leonid shower aboard two aircraft in the 1998 Leonid multi-instrument aircraft campaign and from ground locations in China are presented. Observing at altitude proved particularly effective, with four times higher rates due to low extinction and low angular velocity at the horizon. The rates, derived from a total of 2500 Leonid meteors, trace at least two distinct dust components. One dominated the night of 1998 November 16/17. This two-day wide component was rich in bright meteors with $r = N(m + 1)/N(m) \approx 1.5$ ($s = 1.4$) and peaked at an influx of $3.1 \pm 0.4 \times 10^{-12}$ m^{-2} s^{-1} (for particles of mass $<7 \times 10^{-5}$ g) at solar longitude $\lambda_o \approx 234.52$ (Eq. J2000). The other more narrow component peaked on 1998 November 17/18 at $\lambda_o = 235.31 \pm 0.01$. Rates were elevated above the broad component between λ_o = 235.15 and 235.40, symmetric around the current node of the parent comet 55P/Tempel–Tuttle, peaking at $5.1 \pm 0.2 \times 10^{-12}$ m^{-2} s^{-1}. The population index was higher, $r = 1.8 \pm 0.1$ ($s = 1.7$), but not as high as in past Leonid storms ($r = 3.0$). The flux profile of this component has an unusual asymmetric shape, which implies a blend of contributions from at least two different but relatively recent epochs of ejection. The variation of r across the profile might be due to mass-dependent ejection velocities of the narrowest component. High rates of faint meteors occurred only in an isolated five-minute interval at $\lambda_o = 235.198$, which is likely the result of a single meteoroid breakup in space.

INTRODUCTION

At no other time since the meteor storm of 1966 was there so much interest in the activity of the Leonid meteor shower than in anticipation of the November 1998 return. The Earth was expected to cross relatively recent ejecta of parent comet 55P/Tempel–Tuttle, which returned at perihelion in 1998 February, potentially raising Leonid shower rates above 1/s (Rao, 1995; Yeomans *et al.*, 1996; Jenniskens, 1996). The encounter raised concerns about enhanced collision rates of meteoroids with satellites (Beech and Brown, 1994; Beech *et al.*, 1995; Foschini and Cevolani, 1997) but also raised hopes that such recent ejecta would provide clues to the process of comet mass loss and meteoroid stream dynamics (Jenniskens *et al.*, 1999).

Past accounts of Leonid flux were scrutinized in an effort to anticipate the Leonid returns (Jenniskens, 1995, 1996; Brown *et al.*, 1997; McNaught and Asher, 1999). An observer of such rare and far between events shoulders a twofold responsibility: to satisfy current requirements of the science and to create a reference data base that can be of use in a next time.

NASA's 1998 Leonid multi-instrument aircraft campaign (MAC) was designed to study the Leonid meteors with a wide range of imaging, spectroscopic, and ranging techniques (Jenniskens, 1999; Jenniskens and Butow, 1999). Two aircraft were deployed to Okinawa, Japan, from where the Leonid shower was observed during the night of 1998 November 17/18. To complement the suite of instruments, I contributed a series of intensified video cameras that were intended to provide a record of the meteors detected by other techniques. For example, the cameras would provide low-resolution images of persistent trains and images of meteors for correlation with debris trails detected by the University of Illinois Fe-lidar aboard one of the aircraft. The cameras also provided a record of the meteor flux for studies of the particle size distribution and meteoroid stream dynamics.

These flux measurements are complimented by records from several intensified video cameras at two widely separated sites in China, at plus one and plus two time zones west from Okinawa, which provided flux information at times when twilight prevented further observations from Japan. At those sites, in the provinces of Hebei and Qinhai, observers of the Dutch Meteor Society also obtained rate estimates from visual observations, a traditional source of Leonid rates.

METHODS

In anticipation of perhaps not so stellar meteor rates, I chose to deploy as many cameras as my budget allowed in order to detect sufficient meteors for analysis. Nine new cameras were developed that were flown on FISTA and Electra and one camera was added to three other intensified cameras deployed in China.

I used a proven design consisting of a low f-number objective lens, an AEG multi-channel plate XX1332 second-generation image intensifier, and a Sony CCD-TRV65 Handycam Vision Hi-8 Camcorder that was optically coupled to the intensifier tube (Fig. 1). Two such cameras had been developed earlier, based on the pioneering work by Jobse (1987), and had been used for the purpose of multi-station imaging and flux measurements (Jenniskens *et al.*, 1998). The XX1332 image intensifiers have a large 48 mm photocathode for high spatial resolution and a broad spectral range, which is centered at the V-band photometric filter used to characterize visual magnitudes of background field stars (Fig. 2a). The intensifier photocathode defines the long wavelength response. The short wavelength cut-off is defined by the transmission of the f1.4/50 mm objective lenses (Fig. 2b). The optics of each camera are listed in Table 1. The transmittance of the aircraft windows (Fig. 2b)—three-quarter-inch optical quality BK7 glass on Electra and three-quarter-inch optical quality what may be float glass on FISTA—did not affect the response of the cameras.

Each intensified camera is optically coupled to an NTSC format Hi-8 Camcorder, recording at 30 frames/s, which imprints a time stamp (per one second) in each video frame. The camcorder is mounted only one inch from the intensifier photocathode with almost no image distortion. The camera and intensifier were operated

FIG. 1. Operator Mike Koop with one of the intensified cameras (F300).

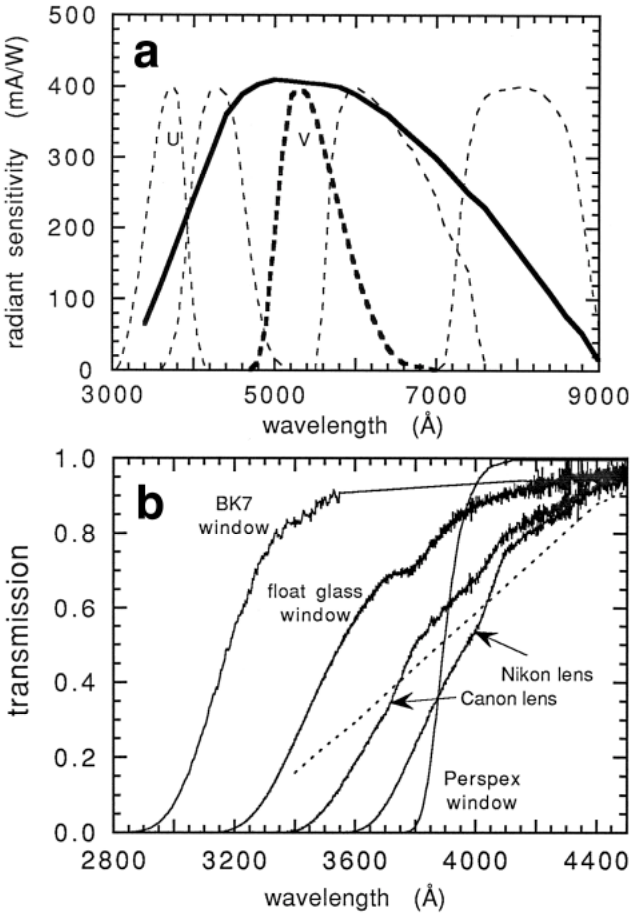

FIG. 2. (a) Radiant sensitivity of the photocathode Type S25 of the XX1332 Intensifiers (factory specification). Superposed are the UBVRI photometric filters (from left to right) used to characterize stellar magnitudes. (b) Measured spectral transmission curves compared to image intensifier photocathode radiant sensitivity (dashed line).

TABLE 1. Intensified cameras.

	Camera optics	Intensifier	Elevation (°)	Field of view (°)	Star-limiting magnitude	N_{tot}	T_{eff} (h)	ZHR/<ZHR>
Electra								
E50F	50 mm f1.4 Canon	XX1332	32	39 × 29	+7.5	360	4.6	0.9
E50R	50 mm f1.4 Canon	XX1332	33	39 × 29	+7.5	245	4.6	0.8
FISTA								
F300	300 mm f2.8 Tamron SP	XX1332	82	7 × 5	+10.0	110	5.7	–
FH55F	55 mm f1.2 Nikon SC	XX1332	36	35 × 26	+7.5	350	5.5	0.9
FH50R	50 mm f1.4 Nikon	XX1332	36	39 × 29	+7*	330	5.9	0.44*
FL50F	50 mm f1.4 Canon FD	XX1332	12	39 × 29	+7.5	1010	5.8	2.2
FL50R	50 mm f1.4 Canon	XX1332	12	39 × 29	+7.5	790	5.8	1.7
FH20	20 mm f2.8D† Nikon AF	XX1332	36	85 × 60	+3	17‡	5.8	–
FL20	20 mm f2.8D† Nikon AF	XX1332	12	85 × 60	+3	23‡	5.8	–
China–Hebei network								
Xing Long	100 mm f2.8 Canon FD	XX1332	22	27 × 19	+8.1	130	2.7	0.32
Lin Ting Kou	50 mm f1.2 Canon	XX1332	68	ϕ 28	+8.5	391	10.3	0.54
China–Qinhai network								
Delingha	25 mm f1.8 Sony	Delnocta-TS	57	ϕ 28	+7.0	277	15.5	0.37
Ulan	55 mm f1.2 Canon FD	SSC 1400	57	ϕ 28	+8.5	233	5.8	0.38

*Higher level of shot noise.
†With Cokin Diffractor Universe special effect filter.
‡Only meteors brighter than magnitude 0.

either from battery (F300 system on FISTA and both cameras on Electra) or from the aircraft 110V power supply (all other systems). The video data were recorded in analog form on 8 mm tapes, which were replaced every two hours.

The impression of meteors on the video camera is much the same as seen by a visual observer. The resolution of 4.6' per line for the camera (with 50 mm focal length optics) compares to ~3' resolution for the dark-adapted naked eye. Moreover, daytime visual observers tend to be sensitive over a similar spectral range: between about 4200 and 7000 Å, sometimes out to 3200–8350 Å, with a peak at 5600 Å. Night-time observers tend to have peak sensitivity slightly shifted towards the ultraviolet, because different sensors in the retina become important (Sidgwick, 1980).

Cameras equipped with low f-number optics are most efficient at detecting meteors. The 50 mm optics combines the benefits of a relatively large field of view for a slow motion across the sensor with a relatively small field of view that prevents too much mixing in of empty sky per pixel. Six 50 mm cameras were deployed, four on FISTA and two on Electra (Table 1). The camera nomenclature in Table 1 and throughout the paper successively lists aircraft, altitude, focal length, and forward or back viewing direction (*e.g.*, FH50R for FISTA, high, 50 mm, rearward).

Figure 3 shows the position of the camera fields in polar coordinates. The zenith is in the center of the plot, whereas the horizon is indicated by a dashed line. In each aircraft, two cameras were pointed at ~35° altitude, whereas one additional set of two cameras on FISTA was pointed at 12° altitude, thus covering most of the sky accessible from one side of the aircraft. Only a small fraction of the whole sky was covered. Adjacent cameras do not overlap.

There is a slight overlap with the high and low cameras on FISTA, but it is small enough to cause negligible error if treated as independent areas. Below 5° altitude are the irregular tops of the cloud cover below the aircraft, which affect the rates in an unknown manner. Here, we will only consider meteors observed above 5° altitude (*i.e.*, excluding the lower quarter of field of view from the low cameras).

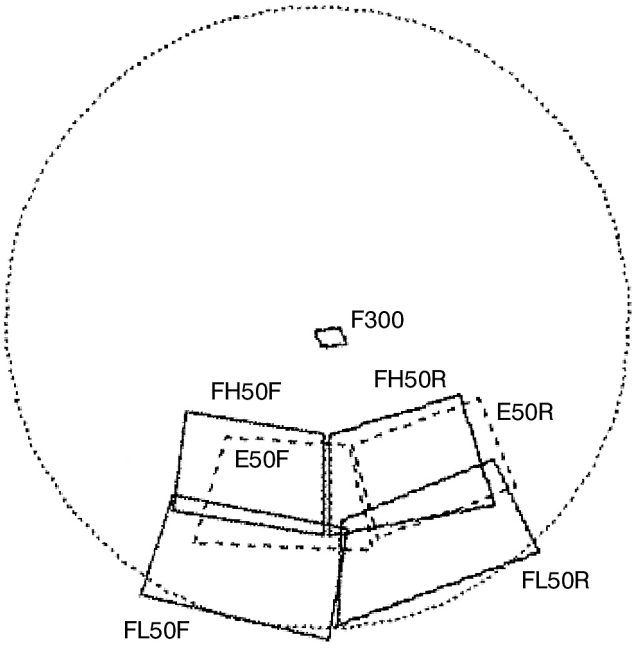

FIG. 3. Camera fields on FISTA (solid lines) and Electra (dashed lines) in altitude and azimuth polar coordinates. The zenith is in the center and the horizon is a dashed circle.

Automatic software exists that can find meteors on video. I installed one of the most advanced software packages, MetRec by Sirko Molau of the International Meteor Organisation, and found that the detection rate was very sensitive to the settings of a number of parameters. Repeated visual inspection always resulted in higher numbers of meteors detected, unless the parameters for a small segment of tape were tuned just right. A demonstration of a second program by Pete Gural of SAIC showed a similar performance. High detection rates are important to arrive at small statistical errors per unit time interval. Hence, I decided to visually inspect all the 50 hours of tapes that were recorded on 1998 November 17/18.

Visual scanning demands extra attention in keeping the detection rate constant. The first inspection typically results in as low as 70 ± 30% of meteors found, with significant variation in efficiency due to the level of concentration at any given moment (Fig. 4). Typically, lapses of concentration do not last long. A second inspection results in better than 90% of meteors detected, with a final <5% variation in detection efficiency from one time interval to the next. Combining rates from all cameras will average out such statistical variations. This defines the detection limit as the sensitivity of the cameras. Amateur observers of the California Meteor Society provided support with the first tape inspection, whereas members of the Dutch Meteor Society examined the tapes from Delingha, Ulan, and Lin Ting Kou (Table 1).

Only those meteors are counted that have their end point in the field of view. This defines the effective field of view as that of the camera, which avoids, for example, over counting early in the night when the trajectories are longer and a meteor is more likely captured in the field of view. The height of the end point is somewhat magnitude dependent and was found earlier to vary between 100 km for meteors of magnitude +6 to 85 km for meteors of magnitude –5 (Jenniskens *et al.*, 1999). If the effect is ignored in influx calculations, rates of +6 magnitude meteors are overestimated by only 15% compared to –5 magnitude meteors. This has a negligible effect in the measured magnitude distribution, because the frequency of +6 and –5 magnitude meteors differs by a factor of 1000.

The aircrafts traveled a pentagon-shaped pattern during the mission at an altitude of 7 km (Electra) and ~13 km (FISTA), turning

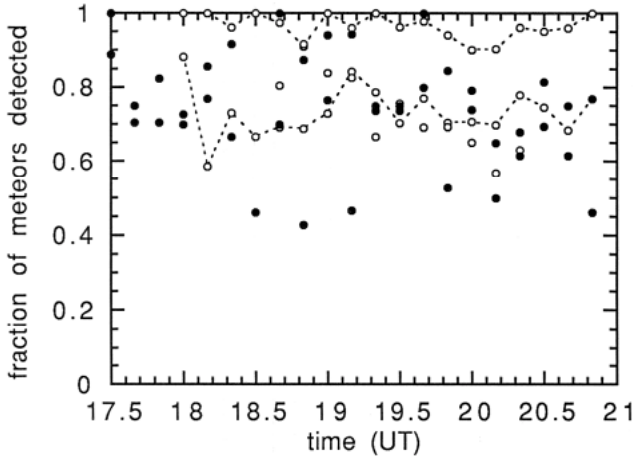

FIG. 4. The fraction of all meteors found during the first inspection of the tapes from high (•) and low cameras (○). The effect of a second inspection is shown by the two dashed lines (data of FL50F), whereas total count includes faint meteors that were not recovered in the second inspection.

about every 20 min in a different direction (Jenniskens *et al.*, 1999). I considered only the periods of time when the camera was stationary with respect to the stars. The periodically changing viewing direction changed the apparent direction of motion of the Leonids in the field of view, which makes it more difficult to recognize the shower meteors in the video record. In order to improve the quality of the shower/nonshower classification, I initially plotted all meteors on gnomonic starcharts of the Brno Gnomonic Atlas (*Lm* = 6.5). All meteors of cameras E50F, E50R, FL50F, and FH50R were thus plotted. I noticed considerable sporadic activity of fast meteors from eastern directions that, when wrongly classified, can affect the rate at early times in the night when apparent Leonid rates are still low. Later in the night, the high number of Leonids makes classification by comparison possible. After recognizing the pitfalls while studying the first cameras, meteors of FL50R and FH50F were classified directly while watching the tapes, with no systematic differences in the flux curves compared to the similar cameras FL50F and FH50R.

Meteor magnitudes were derived by visual comparison with stars in the field of view. Typically, the blooming and apparent intensity of the image of the meteor at its peak brightness is compared to that of stars. Leonids of apparent magnitude +3 and brighter (at 35° altitude) tend to leave a recognizable wake. The faintest Leonids detected on the 50 mm cameras are of apparent magnitude +6.5, ~1 magnitude brighter than the star limiting magnitude (+7.5), as in visual observations. Correction for motion was not applied to the 50 mm images, because no apparent motion is detected for each meteor image. The stellar (V) magnitudes were derived from the Brno Gnomonic Atlas maps. The typical accuracy of magnitude estimates in such visual observations is on the order of ± 0.7 magnitudes.

In order to extend the magnitude range to fainter magnitudes, we deployed one camera with a Tamron *f* 2.8/300 mm lens (shown in Fig. 1), which was aimed close to the zenith to detect intrinsically faint meteors. This camera detected Leonid meteors of apparent magnitude +9. However, each meteor image was distributed over six times as many pixels because of the higher spatial scale on the detector and now appeared as a short band of light. An increase in angular velocity by a factor of 6 leads to an expected loss of 2 magnitudes (Clifton, 1971). Thus, the increased focal length raised the limiting magnitude by only a single magnitude to +7.

Blooming and a lack of comparison stars becomes a serious problem for very bright meteors. In order to correctly estimate the magnitude of meteors brighter than magnitude 0, I used additional cameras with wide angle (20 mm) optics. One such camera was aimed at the same area covered by each set of two 50 mm cameras on FISTA. Each camera has an eight-bit dynamic range, which limits the range of reliable magnitude estimates to about five magnitudes. The wide angle optics was to dilute the meteor signal per

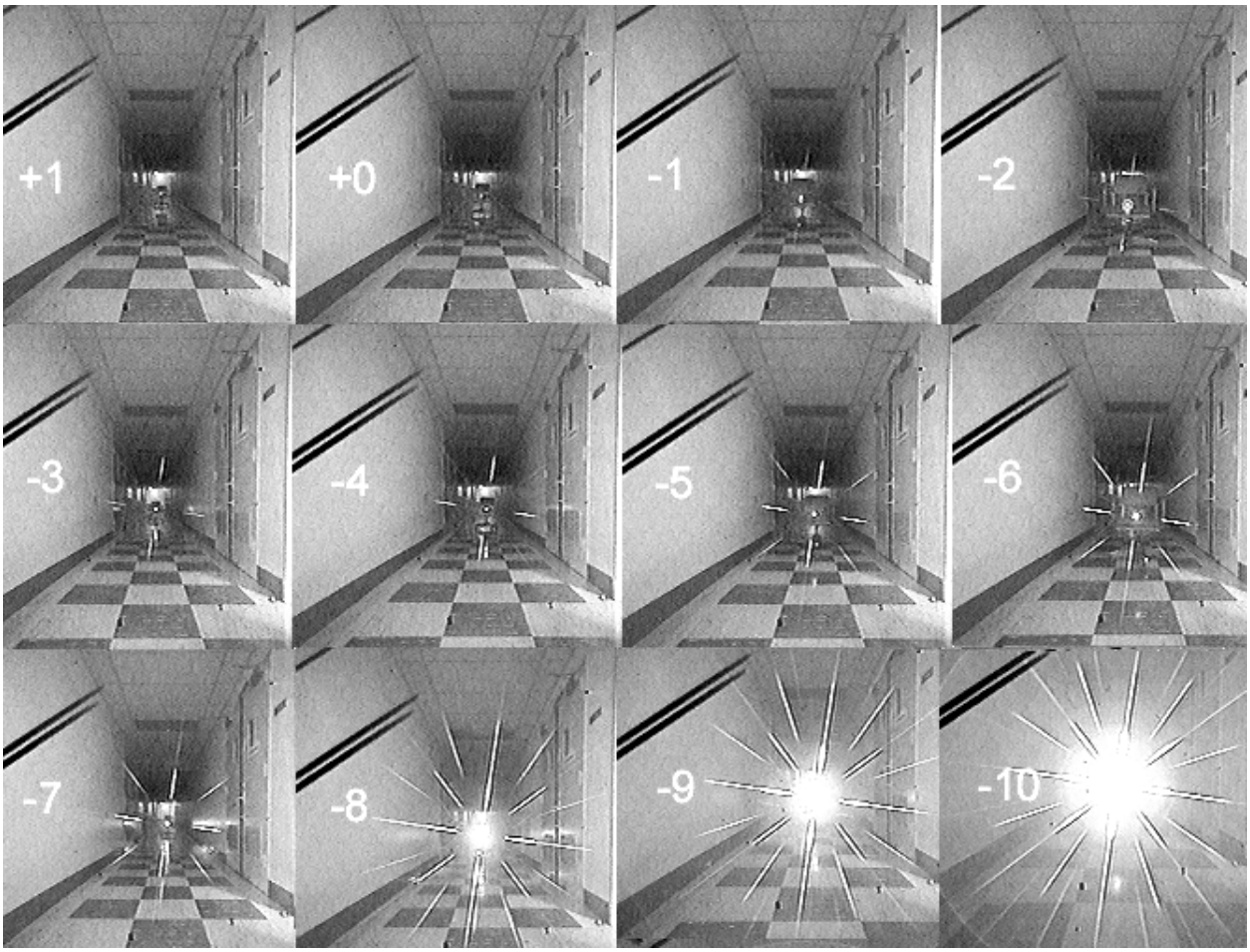

FIG. 5. Calibration of meteor magnitudes from the pattern induced by a low-efficiency diffraction grating (FL20).

FIG. 6. The bright fireball of 18:06:18 UT as observed by the 50 mm (top) and 20 mm (bottom) cameras.

pixel in order to make a different magnitude range accessible in an efficient manner. The limiting magnitude of the 20 mm cameras was about four magnitudes less than that of the 50 mm cameras. In addition, a Cokin Diffractor Universe special effect filter was mounted in front of these cameras, which decreased the limiting magnitude only slightly, but which produced for each magnitude a strikingly different low-efficiency dispersion pattern (Fig. 5). Absolute calibration was achieved by noting how each camera responded to the image of AO type star Sirius (V = –1.5), and the planet Jupter (V = –2.5). Correction for motion was not applied. One result is shown in Fig. 6: the brightest meteor detected by our cameras appeared ~11° above the horizon at 18:06:18 UT and was measured to be of apparent magnitude –9 (absolute magnitude at 100 km distance of –11). A persistent train was imaged for a period of 22 min.

RESULTS

Visual Observations

The 1998 November Leonid shower was arguably the most impressive meteor event since the storm of 1966. Considerable excitement was created by the return of a broad two-day long component rich in bright meteors (Fig. 7) that has been detected in all years since 1994 (Jenniskens, 1996; Brown *et al.*, 1998). The 1995 return was particularly intense with abundant fireballs. An

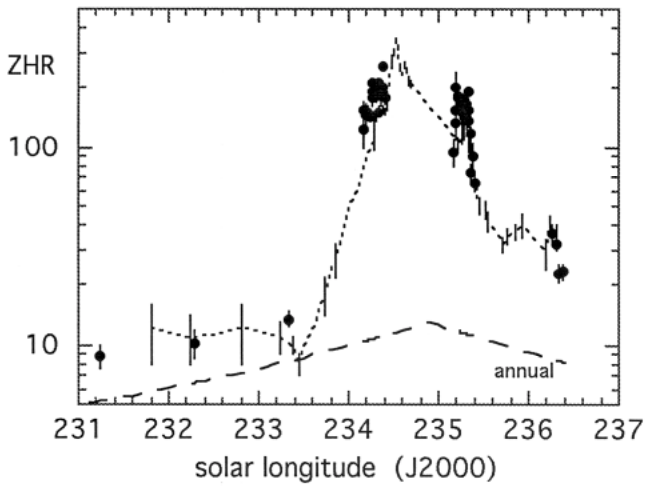

FIG. 7. The 1998 Leonid shower's Zenith Hourly Rate profile measured by visual observers in China (•) and elsewhere (dashed line) (Arlt 1998).

impressive all-sky image of the one European Network station (Modra Observatory, Slovakia) with clear weather, containing 156 meteors brighter than –2 magnitude in a four-hour exposure, testified to the magnitude of the spectacle. On the other hand, initial reports of up to 2000 meteors per hour seen from the Canary Islands turned out to be the result of group counts and, unfortunately, led to the misperception that the expected storm had peaked earlier than predicted.

The first reliable information on meteor flux was provided by visual observers around the globe. They were gathered and processed relatively shortly after the campaign by the International Meteor Organisation. Arlt (1998) found that observers in Europe counted up to zenith hourly rate (ZHR) = 400 meteors per hour at the peak of this bright component (Fig. 7). The ZHR refers to the hourly count of a naked eye observer, after correction for radiant altitude dillution (1/sin (h_r)), for personal perception, and for sky conditions as judged from the star-limiting magnitude (Jenniskens, 1994). A secondary peak in the ZHR profile was detected on 1998 November 17/18 when meteor magnitudes were on average somewhat fainter.

Zenith hourly rate values calculated from counts by visual observers of the Dutch Meteor Society at the ground locations in China (Betlem and van Mil, 1999) agree well with Arlt (1998). It is confirmed that rates at locations in eastern Asia were similar on November 16/17 and 17/8, and rates were still somewhat elevated on the night of November 18/19. It is also confirmed that November 16/17 was dominated by bright meteors, whereas meteors were less abundant on November 17/18. However, our rates for November 16/17 are a little higher than those calculated by Arlt and trace a different profile at the secondary maximum (Fig. 8).

Video Data

In eastern Asia, we were particularly well located to observe any activity variations around the node of the comet orbit, which was at λ_o = 235.258° (Epoch March 8.0, 1998). The time of the predicted maximum was uncertain. Estimates ranged from somewhat before the time of passing the comet node (*e.g.*, the λ_o = 235.20 by Brown and Jones, 1993) to some time after passing the comet node (*e.g.*, the λ_o = 235.338 by Jenniskens, 1996). I hoped that some guidance to the peak time would come from the 1997 observations of the Leonids, but no secondary maximum was observed that year. Langbroek (1999) reported a possible secondary maximum in the

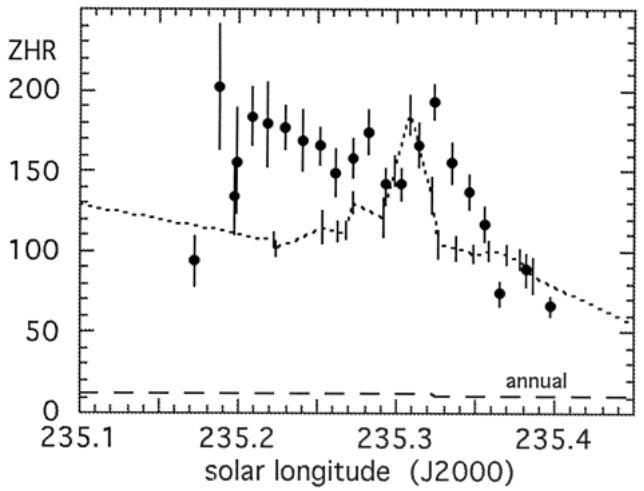

FIG. 8. Detail of Fig. 7 at the secondary peak on the night of 1998 November 17/18.

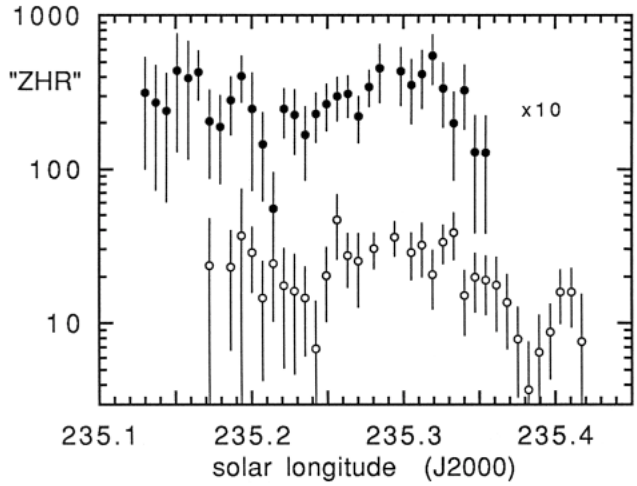

FIG. 9. Video hourly rates "ZHR" from ground-based cameras in Xing Long and Lin Ting Kou of the Hebei network (closed circles, displaced by factor of 10 for visibility) and Delingha and Ulan of the Qinhai network (open circles).

1996 Leonid data, as early as λ_o = 235.172. This seemed to confirm the estimates of Brown and Jones, based on early numerical models, but the actual peak was closer to predictions by Jenniskens (1996), based on past shower observations. Okinawa was chosen as a staging area for Leonid MAC in order to cover all these potential maxima. If the peak would be relatively late, as it was, the observations from China would cover the declining part of the curve.

Let us first examine the video records from ground-based observations in China. A total of 1031 meteors (466 Leonid meteors) from three nights are available for analysis. Let us define a video "ZHR" as the hourly rate of Leonid meteors, corrected for the geometric dilution caused by the radiant altitude (h_r):

$$"ZHR" = N / (T_{eff} (\sin (h_r)) \quad (1)$$

The casual reader should not confuse these rates with the ZHR defined for standard visual observers. No effort is made to take into account the detection limit or spectral response of the instrument, or any other factor that would merely scale the counts. The accuracy of each "ZHR" is limited by the number of meteors (N) in each time interval (T_{eff}). This number is particularly low in the beginning of the night, when the radiant dilution is most severe. The error bars are directly proportional to the root of the number of meteors in each interval:

$$\sigma "ZHR" = "ZHR" / \sqrt{N} \quad (2)$$

Poisson statistics result frequently in significant deviations from the mean. It is this behavior that makes it necessary to observe large numbers of Leonids in each time interval to arrive at precise flux data.

Figure 9 shows the result for the Hebei and Qinhai networks separately. Each curve contains the counts of two camera systems in ten-minute intervals. In the Hebei network, both cameras are independent. In the Qinhai network, both cameras monitor the same part of sky for multi-station work. Even with relatively large error bars, both networks confirm a broad peak of meteors around λ_o = 235.3, and a rapid decline after that.

In comparison to these ground-based observations, the flux measurements from the aircraft proved particularly effective. With similar cameras, two to three times higher rates were recorded by the "high" cameras, whereas the low cameras even picked up 4–6× higher numbers of Leonids. A total of ~3200 meteors (2100 Leonid meteors) from the night of November 17/18 are available for analysis. The low extinction at altitude paid off, especially near the horizon where the effective surface area covered is large. The same type of camera recorded 2–3× higher rates when aimed at 12° rather than at 36°. This came as a real surprise, because predictions made for clear sky ground-based observations predicted rates to decrease towards the horizon (Jenniskens *et al.*, 1999). The calculations did not take into account the very low extinction coefficients at altitude and the lower angular velocity of the meteors near the horizon.

Figure 10 shows the Leonid rates measured from the high cameras aboard Electra and FISTA in ten-minute intervals. If we consider the individual cameras, we note that the cameras for which all meteors were plotted are best sampled and give highest rates, except for the FH50R camera which was hampered by higher shot noise. If we take this into account, we can conclude that all cameras were similarly effective in detecting meteors, independent of azimuthal direction and platform. All cameras recorded highest "ZHR" around λ_o = 235.3, producing peak rates in the early morning, which is consistent with the broad peak in ground-based observations.

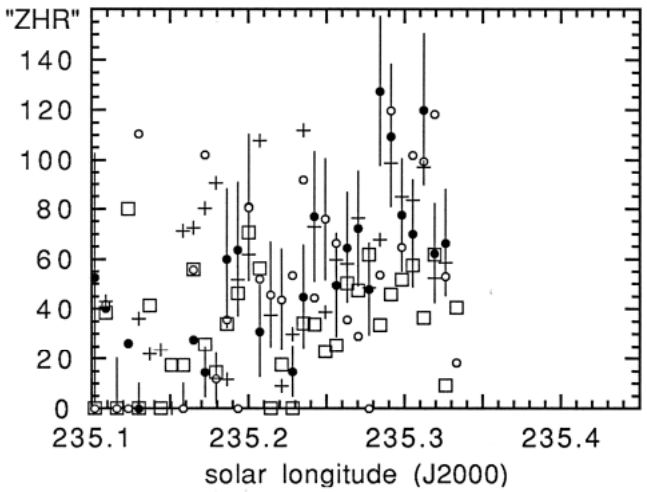

FIG. 10. Leonid rates measured from individual "high" cameras. Symbols: • = E50F, ○ = E50R, □ = FH50R, + = FH50F.

Figure 11 shows the mean Leonid rate of all "high" and all "low" cameras. The latter includes only meteors that ended above 5° altitude. Counts are high enough now to consider five-minute intervals. Again there is a broad peak around λ_o = 235.3. In comparison, sporadic (*i.e.*, nonshower) meteor rates are constant during the night. One high count at λ_o = 235.198 jumps out in a single five-minute interval in both sets of cameras. The jump is followed by a strong decline in rates at λ_o = 235.22 (Fig. 11). Another decline is perhaps seen at λ_o = 235.29. These declines coincide with a viewing direction towards the Leonid radiant, where angular velocities of the meteors are small (Fig. 12).

The lower count in the direction of the Leonid radiant is counter intuitive, because one might expect significantly longer exposure per pixel for meteors that move slower. This is shown in the graphs in Jenniskens *et al.* (1999). However, as already noted in the pioneering work by Clifton (1973), the meteors close to the radiant are not well detected by a visual observer. Recognition of the meteor depends highly on motion. We expect this effect to be strong when the angular velocity is very small. Hence, rates at λ_o = 235.22 are much more affected than rates at λ_o = 235.29. Most affected is camera EF in the interval from 18:08–18:31 UT, when other cameras are also pointed close to the Leonid radiant. We applied a small correction for this time interval, a factor of 1.1 for each affected camera to derive Fig. 13.

Figure 13 combines airborne (full circle = five-minute counts) and ground-based observations (open circles = ten-minute counts), the latter scaled to the airborne data. Note that the two final counts from the airborne campaign are significantly lower than those measured further west, because twilight had arrived in Okinawa.

Population Index

Before examining the shape of the flux profile, one has to consider possible changes in the magnitude population index, $r = N(m + 1)/N(m)$. If the population index is low, then the count is dominated by bright meteors. Less meteors are missed at the detection limit of the instrument. In the case of visual observations, there is also the effect that the effective detection area for bright meteors is much larger (more about that later).

The magnitude distribution of all meteors that were carefully compared with background stars are combined in Fig. 14. The counts for the high 50 mm cameras (circles in Fig. 14) were shifted in magnitude to account for the smaller apparent brightness due to distance. The absolute magnitude is defined as the magnitude of the meteor were it observed at 100 km distance. Extinction by Rayleigh scattering accounts for only a fraction of a magnitude (Jenniskens *et al.*, 1999). The sum amounts to an average shift of +1.6 magnitude for the Electra cameras (full circles) and +1.35 magnitude for the FISTA cameras (open circles).

The (relatively few) bright meteors with apparent magnitude less than –1 (20 mm cameras) were treated in a different manner. Each individual meteor was reduced to absolute magnitudes from the observed height and an assumed altitude of 95 km. Only meteors that appeared above 10° altitude were selected. Hence, the data sample is complete for meteors of magnitude –3 and brighter. The data (crosses in Fig. 14) are scaled to the counts of the high cameras by the ratio of the effective surface areas covered.

Finally, the magnitude distribution of the F300 camera (open squares in Fig. 14) was taken as is: all trails were counted, also those that left the field of view. This can be done without penalty because the trail length does not change much anymore below magnitude +4 (Jenniskens *et al.*, 1999). The rates are simply scaled to those of the high cameras by matching the count of the brightest meteors.

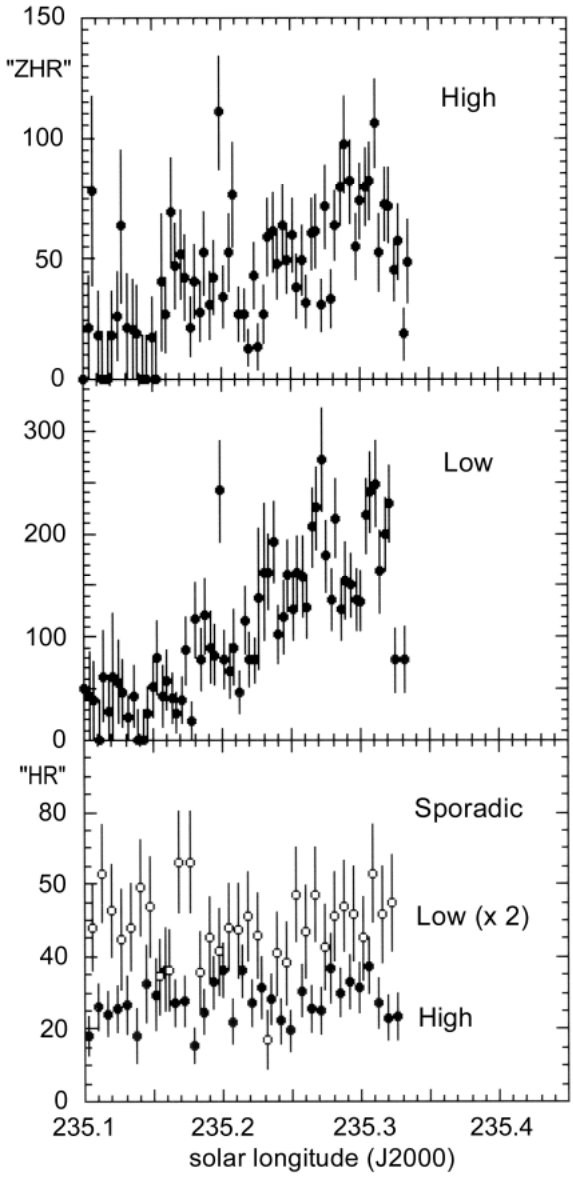

FIG. 11. Five-minute counts of Leonids corrected for radiant dilution. Top graph: high-altitude data; middle graph: low-altitude cameras. Bottom graph shows ten-minute counts of sporadic meteors for high (•) and low (○) cameras (low cameras displaced in solar longitude by +0.003° for clarity).

I find no significant variation of the population index over a wide magnitude range. Although the 50 mm cameras suffer from a decreasing detection efficiency for meteors fainter than +4, the 300 mm camera suggests that counts continue to increase exponentially with magnitude. For the 50 mm cameras, I find that nearly all of +4, 60% of +5, and 19% of +6 Leonids (about one-third of all meteors fainter than magnitude +6.5 are detected). At the same time, 100% of +4, 54% of +5, and 10% of +6 magnitude sporadics (about one-fifth of all meteors are detected).

An exponential curve fitted to the bright meteor tail of a plot of the number of meteors *vs.* magnitude (Fig. 14) results in a mean value of $r = N(m + 1)/N(m) = 1.8 \pm 0.1$ for our Leonids and $r = 2.7 \pm 0.2$

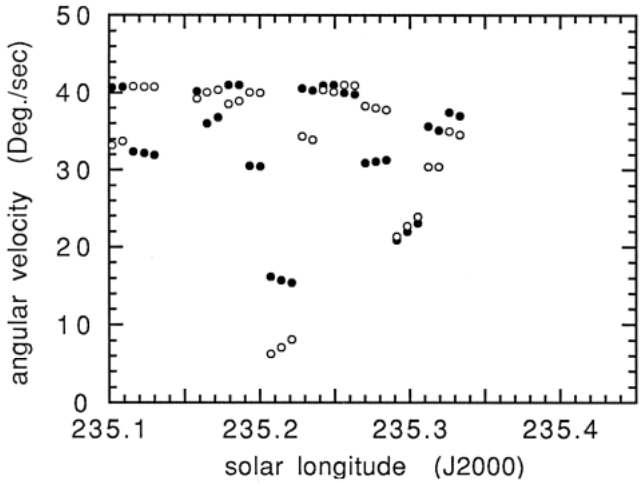

FIG. 12. Angular velocity of meteors in the center of the field of view from the Electra rearward (•) and forward (○) cameras.

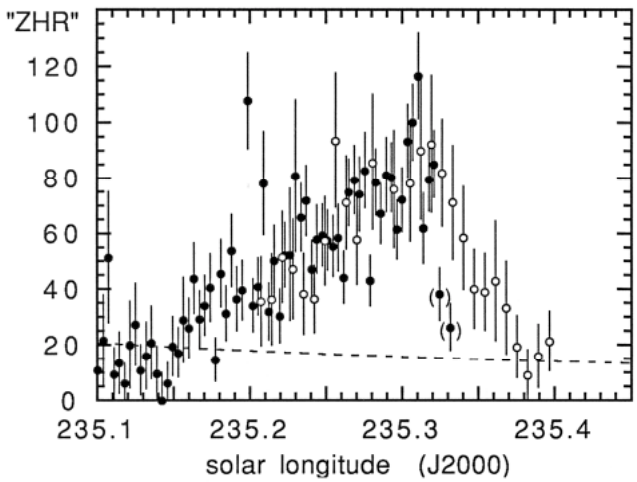

FIG. 13. Mean rates from the aircraft (•) and from the ground (○) (scaled to those of the aircraft).

for the sporadic meteors. The latter value is thought to be $r = 3.4$ (Jenniskens, 1994) and may be less here because of bright Taurid meteors in the sample. A fit to only the 50 mm cameras gives $r = 1.9 \pm 0.1$ for the Leonids.

The variation of population index over the night of November 17/18 is shown in Fig. 15 (open circles are values by Arlt). The observed magnitude distribution in each time interval was corrected for a mean detection probability function $P(m)$, which was derived from Fig. 14 and taken constant during the night. The exponential fit to only the 50 mm cameras was taken, hence the mean of the values in Fig. 15 is at $r \approx 1.9$. The result is 1–3σ variations of r, with low values or $r \approx 1.8$ at the comet node (235.258) and high values of $r \approx 2.4$ at λ_0 = (235.198,) 235.285 and 235.325.

We do not have sufficient meteors detected on the night of November 16/17 (ground data only) to calculate an accurate population index. Arlt derived a population index of only $r = 1.3$ at the peak of this component. Our frequency of Leonid detections on November 16/17 suggests a larger value of r, but not as large as on the night of November 17/18. A value of $r \approx 1.5$ would bring the ZHR values of Fig. 7 down to the observed relative video rates in the nights of November 16 and 17.

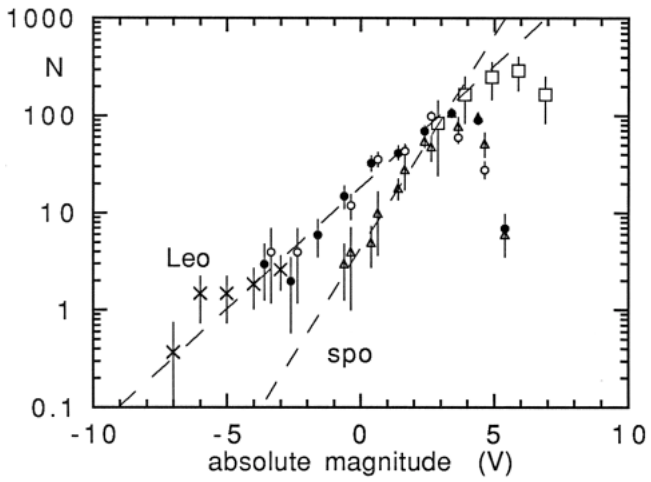

FIG. 14. Magnitude distributions of Leonid and non-Leonid (sporadic) meteors. Symbols: high 50 mm cameras of Electra (•) and FISTA (○), 20 mm cameras of FISTA (×), 300 mm camera on FISTA (□).

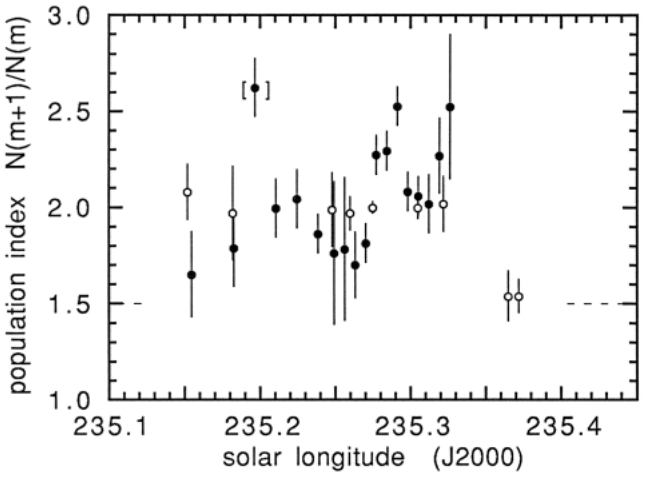

FIG. 15. Population index $N(m + 1)/N(m)$. Closed circles = video data. Open circles = Arlt (1998).

The Influx

The activity scale of Fig. 13 is almost directly proportional to influx. There is a weakly r-dependent correction for meteors missed at the sensitivity limit of the cameras, taken to be (r from Fig. 15):

$$C = (r + r^2) / (0.6 \times r + 0.19 \times r^2) \quad (3)$$

The subsequent scaling involves only the effective observing area. The high 50 mm cameras cover an effective area of 12000 km^2 (Electra) and 8200 km^2 (FISTA). The low camera flux is simply scaled to that of the high cameras. Hence, the sensitivity and spectral response of the high cameras determine the adopted cut off at +6.5 apparent magnitude. From the pointing altitude of the cameras, we have an absolute limiting magnitude of about $V = +5.0$ (mass $\approx 7 \times 10^{-5}$ g). The result is shown in Fig. 16. The peak flux is $5.1 \pm 0.2 \times 10^{-12}$ m^{-2} s^{-1}, in good agreement with calculations from visual observations by Arlt, who derived a value of about 4×10^{-12} m^{-2} s^{-1}.

There is less agreement concerning the intensity of the broad peak (Fig. 17). The step from ZHR to influx consists of one other

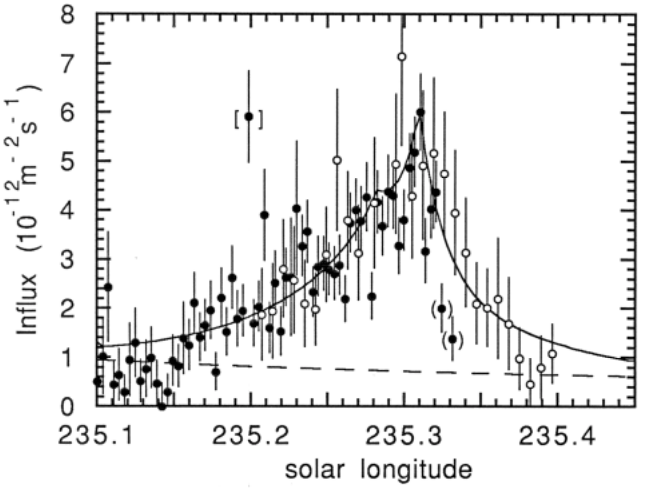

FIG. 16. Meteoroid influx for particles smaller than those producing absolute magnitude +5.0 magnitude meteors (masses less than about 7×10^{-5} g).

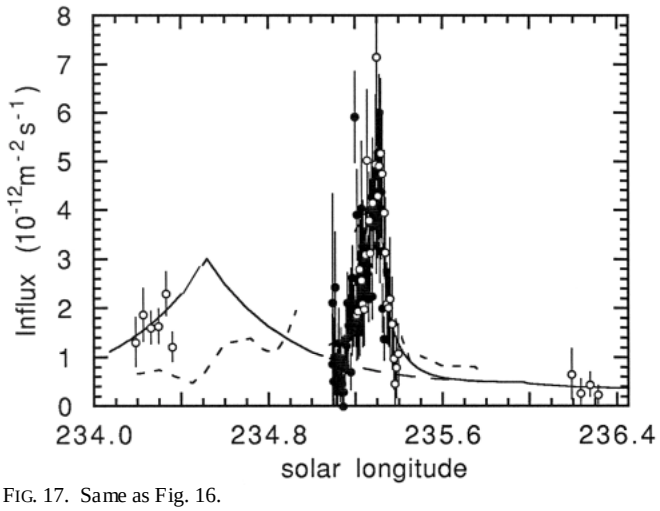

FIG. 17. Same as Fig. 16.

correction in the case of visual observers. The ZHR does not take into account that visual observers pick up bright meteors over a much larger surface area. If that correction is made, the prominent peak in Fig. 7 all but disappears. Indeed, Arlt found the broad component to have negligible flux compared to the "secondary maximum" if meteors <6.5 magnitude are considered (Fig. 17, dashed line).

The video data do not need such correction and define influx independent from the magnitude distribution index, as long as the limit is set above the sensitivity limit of the instrument. Here, we allow for a small correction of rates (Eq. (3)), because the limit is close to +6.5. The ascending slope of the broad component was well observed from China on the night of November 16/17. The dashed line in Fig. 17 is a fit to these data, assuming that the broad background component has the same width as in prior years (*i.e.*, $B = 1.1$; Jenniskens, 1996) and a peak at $\lambda_o = 234.52$ (Arlt, 1998). I find that the broad component over Europe on November 16/17 was not quite as insignificant as determined by Arlt. The peak influx is $3.1 \pm 0.4 \times 10^{-12}$ m^{-2} s^{-1} for particles of mass $<7 \times 10^{-5}$ g. However, I do confirm that the dominant influx occurred over eastern Asia in the next night of November 17/18.

DISCUSSION

A surprising result is the asymmetric shape of the flux profile of the secondary maximum (Fig. 16). The profile is characteristically non-Gaussian and non-Lorenzian. No other meteor outbursts are known to show such behavior (Jenniskens 1995), and ejection mechanisms or planetary perturbations are not expected to cause such asymmetry.

Recent models of the Leonid meteoroid stream (Asher, 1998; Asher *et al.*, 1999; McNaught and Asher, 1999) have drawn attention to small-scale structure in the meteoroid stream that represent individual ejecta deposited at the different returns of the comet. In each return, the orbit of the comet has changed slightly as a result of planetary perturbations and, therefore, the ejecta of large submillimeter-to-centimeter sized grains are deposited in slightly different orbits. Over time, the dust continues to spread out along the comet orbit in a trail-like structure, due to small orbital period variations from one dust grain to the next; and planetary perturbations on individual orbits tend to disperse the trails gradually. Until recently, it was assumed that the ejecta of all epochs would merge into a single dust trail. Now, it is believed that individual returns can be recognized when Earth passes these relatively recent ejecta.

Our data provide the outline of a narrow dust component superposed on the broad component and the annual stream background. A similar peak was observed during the return of 1965, and the whole shower profile is very reminiscent of that return (McIntosh and Millman, 1970; Jenniskens, 1996). The narrow peak is much wider than typical for Leonid storms, which have a characteristic ($2 \times 1/e$) width of $\Delta\lambda_o = 0.029°$ (Jenniskens, 1995). The profile of Fig. 13 has a width of 0.14°.

The puzzling asymmetry and relative large width suggests that this profile is a composite of at least two, and perhaps as many as four, more narrow features. A good fit needs at least two symmetric components of the characteristic form (Jenniskens, 1995):

$$"ZHR" = "ZHR_{max}"\ 10^{(B\,|\,\lambda_o{}^{max} - \lambda_o\,|)} \qquad (4)$$

The fit shown in Fig. 16 has a narrow component fitted to the steep declining branch of the curve. The parameters of this component correspond to $B \approx 30$ and peak at $\lambda_o = 235.31$, so chosen because the width is that of past Leonid storms (Jenniskens, 1995). A broader background with $B = 6$ was identified in these profiles also (Jenniskens, 1995, 1996), and I find that the rest of the curve is indeed well fitted by a component with $B = 6 \pm 1$ and $\lambda_o = 235.280 \pm 0.005$. This part would contain 6–30× as much mass if the size distribution is identical. Note that while in other years the $B = 6$ component provided a background to the main peak, this time the components seem to be separated.

I have no strong evidence for the presence of a narrow component having the high $r = 3.0$ of past meteor storms. At first sight, the lack of a storm prevents us from studying the mass-dependent ejection velocities of large cometary grains. On the other hand, the two peaks of high $r \approx 2.4$ at $\lambda_o = 235.29$ and 235.325 in Fig. 15 could be the anticipated signature of particle-size-dependent ejection velocities. Just such time dependence would be expected if superposed on a component rich in bright meteors; there is one with the small particles being dispersed further out than the large grains. Such a scenario can only be confirmed by numerical models, which are beyond the scope of this paper.

The spike at $\lambda_o = 235.198$ in Fig. 15, with high numbers of faint meteors, corresponds to a narrow spike in the flux curve. This spike is so brief in duration that it is probably caused by a single frag-

mented meteor, much as in the brief burst of Leonids observed during the 1997 return by Kinoshita *et al.* (1999). Except, in this case, the fragmentation occurred further back in time.

CONCLUSION

For the first time, a large enough number of video cameras were deployed in a single experiment and under excellent observing conditions to provide sufficient numbers of meteors for a statistically significant detection of structures in the meteor shower activity curve from video records.

The flux measurements are in good agreement with those of visual observers. The video data make it possible to better estimate the relative influx of the broad component of bright meteors and the narrow "secondary" peak. I confirm that the last is the more important at small particle sizes.

The video data are precise enough to recognize an asymmetric "secondary" peak shape.

Our observations are consistent with the Earth meeting successive ejecta of different epochs. There is no filamentary structure with large variations in maxima and minima. Rather, the flux curve is composed of a number of debris components that have blended. A direct comparison with theory may allow the identification of the epoch of ejection of each component, but such work is outside the scope of this paper.

Acknowledgments–Many people contributed to the success of this experiment. The cameras were developed with financial support of NASA Ames Research Center's Director's Discretionary Fund. Gary Palmer of EM Engineering constructed the hardware, and Mike Koop of Lockheed-Martin provided the electronic circuits. We thank FISTA and Electra operators who helped install the cameras. Special thanks goes to Norm Zrubrek of the NCAR Research Aviation Facility in Broomfield. Mike Koop operated the cameras onboard FISTA, with help of Steve Butow, while Mike Wilson assisted in the operation onboard Electra. NASA's Leonid MAC was supported by NASA Ames Research Center and by NASA's Planetary Astronomy Program, Exobiology Program, and the Astrobiology Advanced Missions and Technology program. Jane Houston, Morris Jones, Mark Taylor, and Bob Elsberry of the California Meteor Society (CMS), and intern David Nugent helped scan the video tapes. The video cameras at the ground site in China were owned and operated by Dutch Meteor Society members Carl Johannink and Casper ter Kuile (station Ulan), by Romke Schievink (Delingha), and by Klaas Jobse (Lin Ting Kou). California Meteor Society member Ming Li operated the Xing Long camera and helped coordinate the effort. I thank Hans Betlem and Olga van Mil who provided a summary of ground-based visual observations, and Carl Johannink for his research into the video data. Financial support for the ground-based campaign was provided by the Dutch and Chinese Academies of Sciences, the Leids Kerkhoven-Bosscha Fonds, and the NASA Planetary Astronomy program.

Editorial handling: D. W. G. Sears

REFERENCES

ARLT R. (1998) Bulletin 13 of the International Leonid Watch: The 1998 Leonid Meteor Shower. *WGN, J. IMO* **26,** 239–248.

ASHER D. J. (1998) The Leonid meteor storms of 1833 and 1966. *Mon. Not. R. Astron. Soc.* **307,** 919–924.

ASHER D. J., BAILEY M. E. AND EMEL'YANENKO V. V. (1999) Resonant meteoroids from Comet Tempel–Tuttle in 1333: The cause of the unexpected Leonid outburst in 1998. *Mon. Not. R. Astron. Soc.* **304,** L53–L56.

BEECH M. AND BROWN P. (1994) Space platform impact probabilities—The threat from the Leonids. *ESA J.* **18,** 63–73.

BEECH M., BROWN P. AND JONES J. (1995) The potential danger to space platforms from meteor storm activity. *Q.J. R. Astr. Soc.* **36,** 127–152.

BETLEM H AND VAN MIL O. (1999) Leoniden 1998 Visuele Resultaten. *Radiant, J. Dutch Met. Soc.* **21,** 65–72.

BROWN P. AND JONES J. (1993) Evolution of the Leonid meteor stream. In *Meteoroids and Their Parent Bodies* (eds. J. Stohl and I. P. Williams), pp. 57–60. Astronomical Institute, Slovak Acad. Sci., Bratislava, the Slovak Republic.

BROWN P., SIMEK M. AND JONES J. (1997) Radar observations of the Leonids: 1964–1995. *Astron. Astrophys.* **322,** 687–695.

BROWN P., SIMEK M., JONES J., ARLT R., HOCKING W. K. AND BEECH M. (1998) Observations of the 1996 Leonid meteor shower by radar, visual and video techniques. *Mon. Not. R. Astron. Soc.* **300,** 244–250.

CLIFTON K. S. (1971) *Airborne Meteor Observations at High Latitudes.* NASA Technical Note D–6303, Marshall Space Flight Center, Alabama, USA. 49 pp.

CLIFTON K. S. (1973) Television studies of faint meteors. *J. Geophys. Res.* **78,** 6511–6521.

FOSCHINI L. AND CEVOLANI G. (1997) Impact probabilities of meteoroid streams with artificial satellites: An assesment. *Il Nuovo Cimento, Note Brevi* **20,** 211–215.

JENNISKENS P. (1994) Meteor stream activity I. The annual streams. *Astron. Astrophys.* **287,** 990–1013.

JENNISKENS P. (1995) Meteor stream activity II. Meteor outbursts. *Astron. Astrophys.* **295,** 206–235.

JENNISKENS P. (1996) Meteor stream activity III. Measurement of the first in a new series of Leonid outburst. *Meteorit. Planet. Sci.* **31,** 177–184.

JENNISKENS P. (1999) Update on the Leonids. *Adv. Space Res.* **23,** 137–147.

JENNISKENS P. AND BUTOW S. (1999) The 1998 Leonid multi-instrument aircraft campaign—An early review. *Meteorit. Planet. Sci.* **34,** 933–943.

JENNISKENS P., BETLEM H., DE LIGNIE M., TER KUILE C., VAN VLIET M. C. A., VAN 'T LEVEN J., KOOP M., MORALES E. AND RICE T. (1998) On the unusual activity of the Perseid meteor shower (1989–96) and the dust trail of comet 109P/Swift–Tuttle. *Mont. Not. R. Astron. Soc.* **301,** 941–954.

JENNISKENS P., DE LIGNIE M., BETLEM H., BOROVICKA J., LAUX C. O., PACKAN D. AND KRUEGER C. H. (1999) Preparing for the 1998/99 Leonid Storms. In *Laboratory Astrophysics and Space Research* (eds. P. Ehrenfreund, C. Krafft, H. Kochan and V. Pirronello), pp. 425–455. Kluwer Academic Publishers, Dordecht, the Netherlands.

JOBSE K. (1987) Betsy. *Radiant, the Journal of the Dutch Meteor Society* **9,** 83–84.

LANGBROEK M. (1999) Leonid outburst activity 1996: A broad structure and a first occurrence of a narrow peak of fainter meteors. *Meteorit. Planet. Sci.* **34,** 137–145.

KINOSHITA M., MARUYAMA T. AND SAGAYAMA T. (1999) Preliminary activity of Leonid meteor storm observed with a video camera in 1997. *Geophys. Res. Lett.* **26,** 41–44.

MCINTOSH B. A. AND MILLMAN P. M. (1970) The Leonids by radar—1957 to 1968. *Meteoritics* **5,** 1–18.

MCNAUGHT R. H. AND ASHER D. J. (1999) Leonid Dust Trails and Meteor Storms. *WGN, J. IMO* **27,** 85–102.

RAO J. (1995) The Leonids: King of the Meteor Showers. *Sky & Telescope* **90,** 24–31.

SIDGWICK J. B. (1980) *Amateur Astronomer's Handbook*. 4th ed. Enslow Publishers, Hillside, New Jersey, USA. 568 pp.

YEOMANS D. K., YAU K. K. AND WEISSMAN P. R. (1996) The impending appearance of Comet Tempel–Tuttle and the Leonid Meteors. *Icarus* **124,** 407–413.

Forward
Back
Table of Contents